SAND2001-8022C

Evaluation of NH_4F/H_2O_2 Effectiveness as a Surface Passivation Agent for $Cd_{1-x}Zn_xTe$ Crystals

G.W. Wright[1,2], R.B. James[1], D. Chinn[1], B.A. Brunett[1], R.W. Olsen[1], J.Van Scyoc III[1], M. Clift[1]
A. Burger[2], K. Chattopadhyay[2], D. Shi[2], R.Wingfield[2]

[1]Sandia National Laboratories, P.O Box 969, Livermore, CA 94551
email: **wrightway7@yahoo.com**

[2]NASA Center for Photonic Materials and Devices,
Fisk University, Nashville TN 37208

Abstract

Various passivating agents that reduced the surface leakage current of CZT crystals have been previously reported. In one of the studies, NH_4F/H_2O_2 was identified as a promising passivation agent for CZT. We now present a study that includes the effect of NH_4F/H_2O_2 treatment on the surface properties and detector performance. An elemental depth profile was obtained via Auger Electron Spectroscopy. Furthermore, X-ray Photoelectron Spectroscopy acquired at different processing times to identify the chemical states of the elemental species that composed the dielectric layer. It was found that the NH_4F/H_2O_2 surface passivation significantly improved the sensitivity and energy resolution of CZT detectors. Furthermore, the NH_4F/H_2O_2 treatment did not attack the Au electrodes, which eliminated the need to protect the contacts in the detector fabrication process.

1. INTRODUCTION

The process of surface passivation of Cadmium Zinc Telluride (CZT) detectors has been explored by many laboratories, in parallel with other efforts for the optimization of the crystal growth process[1-9]. The electrical properties of polycrystalline CZT are mitigated by bulk and surface grain boundaries. In addition, dangling bonds, and non-stoichiometric surface species produce defects that are responsible for high surface leakage current. Passivation of the semiconductor is needed to decrease the surface leakage current, and thereby, improve detector performance. The improved detector sensitivity and resolution can be identified by an increased signal-to-noise ratio, increased peak-to-valley ratio, and decreased Full-Width-Half-Maximum (FWHM). In this paper the reductions in surface leakage current after surface passivation are shown. We have chosen to use the low energy X-ray peaks of Am^{241} to demonstrate the reduction of leakage current as indicated by photopeak narrowing (FWHM) and increases in peak-to-valley ratios.

Passivation is a chemical and/or physical process that renders the surface of a material chemically and/or electrically inert to its environment. The chemical and/or physical processes employed produces reaction products either directly with the surface of the semiconductor, or via the deposition of a different material, which has the suitable properties that will passivate the semiconductor surface. Passivation can be facilitated by proper surface treatment via a stoichiometric etch, deposition of dielectric materials, or by the formation of dielectric reaction products (native films) at the surface of the semiconductor.

In the technology of passivation, we first try to produce a surface that is stoichiometric with a minimum number of electrically active defects. Secondly, the reacted layer should be uniform and have good physical adherence. Finally, the reacted layer should provide a barrier that will prevent the diffusion of reactive species to the surface of the semiconductor. The last effect provides for long term, stable detector operation. The film must also be thermodynamically stable with its environment and the surface of the semiconductor that lies below the electrode. Otherwise, films can be grown from the surface of a semiconductor, which may react with the environment or with the semiconductor itself. For example, the occurrence of oxides on GaAs (Ga_2O_3 and As_2O_3), whereby the following reaction takes places: $2GaAs + As_2O_3 \rightarrow Ga_2O_3 + 4As$. The arsenic oxide is thermodynamically unstable in the presence of GaAs and as a result produces an oxide that is a matrix of Ga oxide with elemental As. In this case, the thermal and chemical stability of the dielectric layer is compromised because of chemical reaction between the dielectric layer and the semiconductor surface.

Passivation of CZT is complex because it is a ternary compound, with each of its chemical constituents having different chemical properties, and there is a tendency for electrically active defects to form at the interface region during the passivation process. In order to make high quality devices, it is essential and critical to form stable and reproducible passivated surfaces, with well-controlled electrical properties.

The processing of the as grown semiconductor crystal requires passivation of the semiconductor surface. During processing, the crystal is cut to appropriate dimensions. Then, depending on the application of the material, it may be necessary to remove the damage due to cutting. Mechanical polishing or lapping follows to produce flat planar surfaces. After mechanical polishing there may be some residual mechanical damage left on the semiconductor surface. The mechanical damage produces surface states. To reduce the number of surface states on the surface of the semiconductor, the surface of the semiconductor often undergoes a chemical processing step. The chemical etching is implemented to remove as many surface states as possible by restoring the stoichiometry and crystallinity of the near surface region. In the silicon industry it was found that in order to achieve a low density of surface states the SiO_2/Si interface had to have the following conditions: (a) a reduction of dangling bonds on the silicon surface, (b) reduced bond angle disorders, (c) a lower concentration of dangling Si and Si-Si bonds in the oxide, (d) less stretched Si-O and Si-Si bonds, and (e) fewer trivalent Si-Si bonds. All of the aforementioned precursors to surface states are the results of mechanical damage due to cutting and polishing of the crystal. Non-stoichiometric chemical etching of the surface can also leave surface states for compound semiconductors.

Furthermore, the deposition of dielectric layers by chemical vapor deposition (thermal and plasma-enhanced) or by sputtering generally exhibit a large density of interface states. Dielectric layers grown thermally or via a wet chemical approach normally exhibit a low density of interface states. A large density of interface states can be detrimental to the insulating properties of the dielectric layer. Interface states provide a mechanism for tunneling of carriers through barriers. For example, if these interface states are neutral, they can trap a specific carrier depending on the polarity of the bias applied at the metal contact. The trapped carriers at the interface introduce a charge that distorts the electric field in the semiconductor. Moreover, if the applied bias is reversed to repel the carrier type trapped at the interface, the carriers can tunnel out of the insulator states into the detector. Tunneling carriers could be responsible for an increase in dark current noise, leakage current, and electrical contact breakdown in detectors fabricated from CZT. As a result of the opportunity for charge buildup and tunneling via interface states between the oxide and the nonstoichiometric CZT, metal contacts with an interfacial oxide layer can be detrimental to detector performance at negative bias[11,12].

In order to control the electrical properties of the interfaces, it is usually adequate to form an approximately 2 nm native film[4]. However, to consume a sufficient amount of the semiconductor surface such that the semiconductor surface is etched, a 20-30 nm native dielectric layer should be produced from the semiconductor surface[4]. Etching is very important to remove the surface layer damaged from the various processing techniques utilized in device fabrication.

The native insulating layer has the following three effects. First, it controls the surface electrical properties of the semiconductor by fixing the surface potential with fixed interface charges. Second, it reduces the density of surface states that are otherwise observed in the disordered surface region. Finally, the growth process of the native film consumes the CdZnTe surface layer (i.e. dangling bonds), which is possibly damaged and nonstoichiometric, in a controlled manner.

2. EXPERIMENTAL

2.1 SAMPLE PREPARATION

The CZT samples were mechanically polished using 0.5 micron alumina powder, followed by a subsequent dip in reagent grade bromine/methanol etch for 1 minute at room temperature on each side of the sample. Each CZT sample was rinsed twice in methanol and dried in air prior to the metalization process.

Two methods of metalization were used for the application of the electrical contacts: 1.) RF plasma sputtering of Au contacts in vacuum utilizing a Kurt J. Lesker RF sputtering system operated at 50 Watt power and; 2.) electroless gold deposition. Electroless deposition of Au became the method of choice in order to expedite device fabrication. Photolithography with contact masks and liftoff processing were utilized to pattern Au contacts on CZT.

Following the metalization process, the electrical leads of Pt wire were attached to the Au contact with an Aquadag conductive adhesive to ensure a good electrical connection between the Pt wire and Au contact. The attached Pt wire was

DISCLAIMER

sealed to the Au metal contact with a polymer encapsulant of Humiseal. The Humiseal helps to ensure the mechanical stability of the Pt wire-Au contact connection.

2.2 EXPERIMENTAL PROCEDURE

25 ml of 10%wt NH_4F 10%wt H_2O_2 aqueous solutions were prepared and poured in 100 ml beakers. The CZT samples were then placed in the solution for 5 minute intervals. Three consecutive dips of each sample were performed. After each dip, an I-V curve was obtained utilizing a Bertan high voltage power supply Model 225 and a Keithley electrometer Model 617, both interfaced with a PC. From the I-V curves we can find the optimal passivation time needed to minimize the surface leakage current.

The samples were immersed in chemical treatments of 10%wt NH_4F 10%wt H_2O_2 according to their respective optimal dip time. Spectral measurements were taken using a conventional nuclear spectrum acquisition system consisting of a preamplifier, linear amplifier, and multichannel analyzer. After drying in argon and subsequent drying in air for 2 hours, the I-V curves and detector spectrum were taken again. Plots of I-V curves and corresponding spectra were remeasured. The percent reduction of leakage current, improvement factor of resistance, and resistance were calculated.

2.3 DETECTOR FABRICATION

The detector fabrication method shown in Figure 2.1 is the process utilized to acquire the I-V results presented in this paper. The attached electrical leads are protected with the insulating polymer, Humiseal, to ensure mechanical stability of the wire to the metal electrode.

It was demonstrated upon further experimentation that the chemical process that produced the passivation layer did not attack either the positive photoresist or the electroless Au electrode. This allowed us to eliminate two of the steps in a photolithography process for protecting the patterned electrode. Thus, we could deposit a patterned electrode on the CZT crystal, and then passivate the crystal without protecting the electrode area from the passivation process. This detector fabrication method is illustrated in Figure 2.2. The before and after NH_4F/H_2O_2 passivation detector response utilizing this fabrication method is discussed in section 3.4 of this paper.

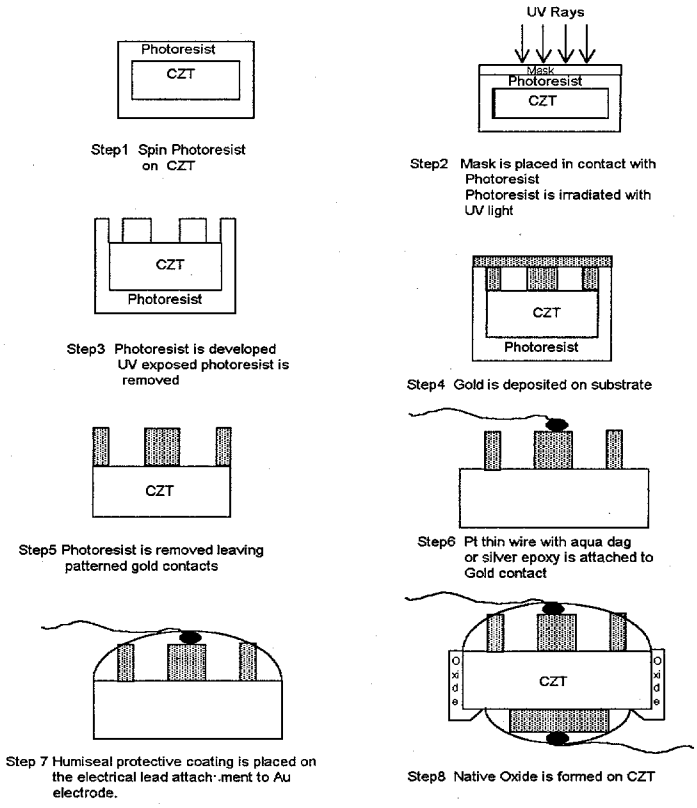

Figure 2.1 Protected gold electrode fabrication method used for detector measurements.

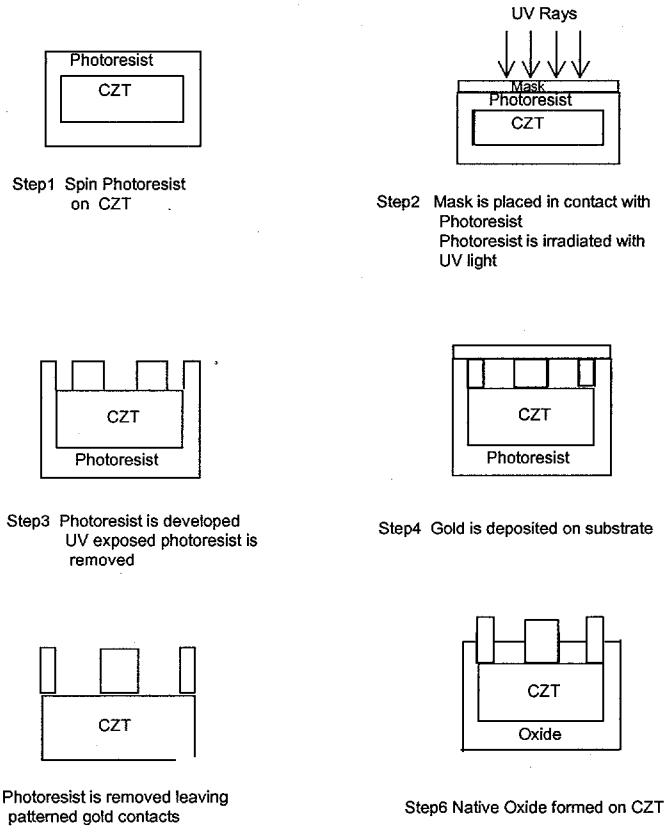

Figure 2.2 Unprotected gold electrode fabrication method used for detector measurements.

3. RESULTS

3.1 (AES) AUGER ELECTRON SPECTROSCOPY

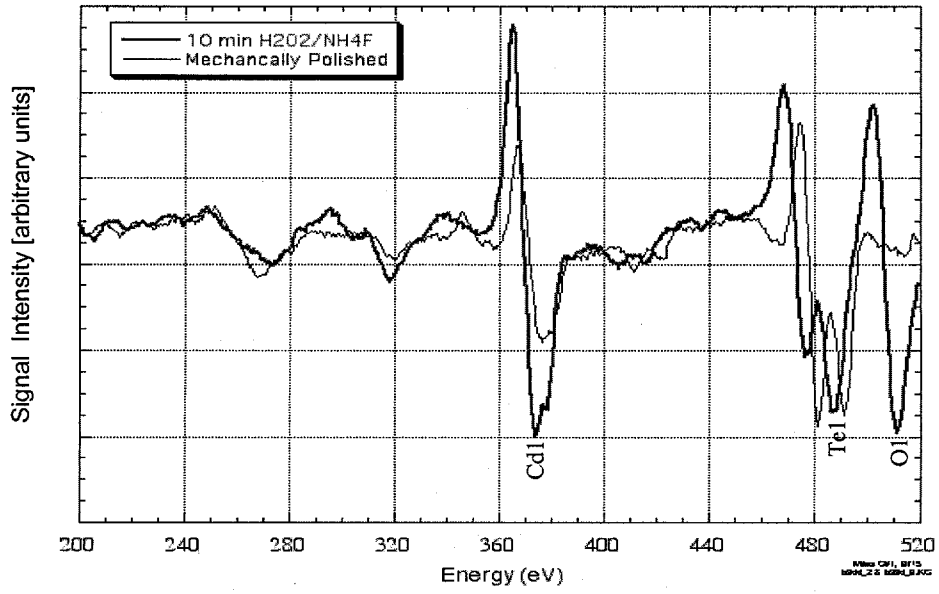

Figure 3.1 Comparison of a mechanically polished CZT sample with a CZT sample that was etched for 10 min in a H_2O_2/NFH_4F solution. Note the appearance of the oxygen peak after NH_4F/H_2O_2 treatment with a corresponding change in the shape of the Cd and Te peaks. Furthermore, the Auger electrons from Cd and Te have less kinetic energy indicating that their chemical state has changed. The amount of shift to lower kinetic energy indicates that Cd and Te have been converted to CdO and TeO_2.

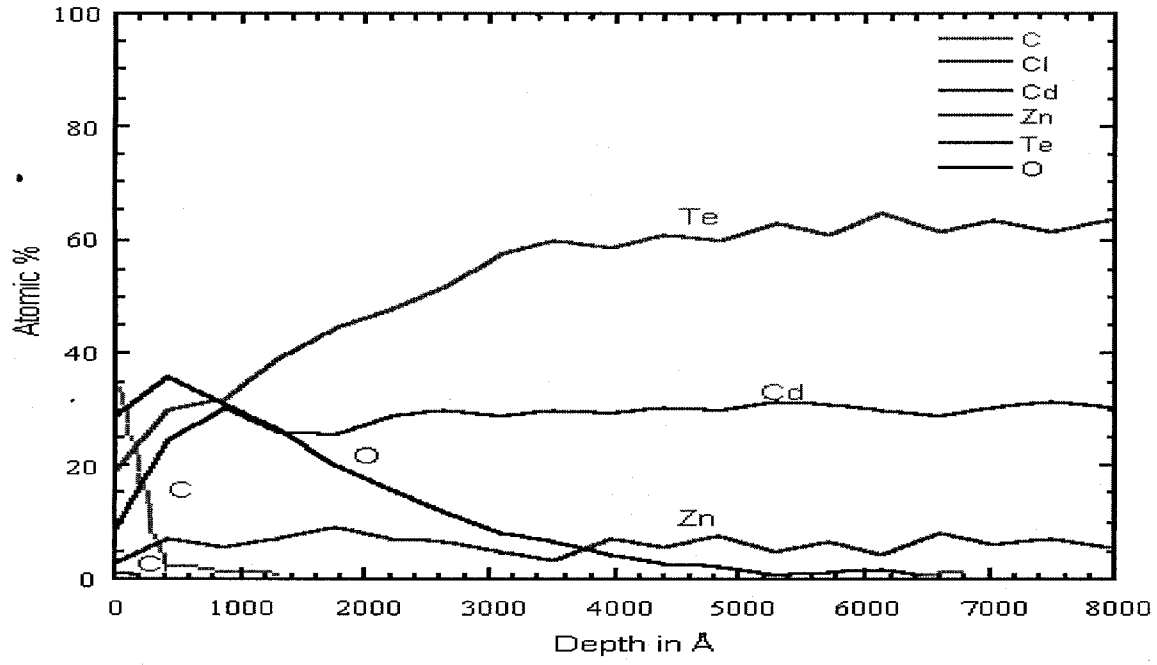

Figure 3.2 Auger depth profile of CZT exposed to the H_2O_2/NH_4F solution. Note that the scale for depth in Å is not precisely calibrated. We do not currently know the Ar sputter rate of this oxide and chose to use the same sputter rate as SiO_2 under the same conditions.

We are currently trying to quantify the oxide thickness using surface profilometry and ellipsometry. The results indicate an initial layer of CdO with a layer of TeO_2 covering it. X-ray Photolectron Spectrsocopy (XPS) was used to study the chemical composition of the layer. A mechanism for formation of this dielectric layer is proposed in the discussion section of this paper.

3.2 X-RAY PHOTOELECTRON SPECTROSCOPY

For Te there is the appearance of a new peak at higher binding energies after passivation. The new peak location is at the expected binding energy for Te when it is in the chemical state as TeO_2. The peak for Te $3d_{5/2}$ before passivation was at 573.2 eV. A new peak appearing after immersion in passivation solution was at 576.5 eV. There is also a correlation between the decrease in the peak at the Te level and a corresponding increase in the peak intensity at the TeO_2 level. The aforementioned result indicates that the Te on the surface is being consumed and converted to TeO_2 with residual Te still present deep in the oxide layer. It should be noted that in previous published papers there is little or no correlation between the reduction in the Te peak and the appearance of a TeO_2 peak[9], suggesting that the oxidation of excess Te was incomplete in those papers. Moreover, it was reported a $CdTeO_3$ related oxide, which is probably a salt, was present[9]. We have observed no other related Te compounds on the surface such as nitrates, other oxides of Te, or fluorides.

For Cd there is a peak at 405.0 eV. After passivation for 3 minutes, the peak for Cd shifts to higher binding energies. The new peak location is at 405.3 eV. The new peak location is at the binding energy for Cd when Cd is in the chemical state as CdO. The peak shift of 0.3 eV is the exact amount indicated for the conversion of Cd in CdTe to CdO. The intensity of the oxygen peak at 530 eV follows the exact same behavior as the CdO peak at 405.3 eV. We observe no other related Cd compounds on the surface such as nitrates, selenides, sulfides, or fluorides.

The binding energy peak for carbon was utilized to correct for the effects of charging. A true depth profile can not be accomplished without sputtering. In XPS the incident beam of X-rays is normally perpendicular to the sample allowing for the greatest depth of the dielectric layer to be analyzed. However, by tilting the sample from its normal horizontal position to 30^{O}, then 60^{O} we can vary the amount of the dielectric layer analyzed. The greater the tilt, the smaller the amount of dielectric layer is sampled. Because the sampling depth in XPS is only .5 to 5 nm, as compared with the AES depth profile which could be 100 nm, we are only able to obtain a qualitative depth profile by sampling a 5 nm slice of the dielectric layer at different times.

In order to obtain a qualitative depth profile of the dielectric layer, three different CZT samples were analyzed after passivation for different times. The first sample used a traditional Bromine/Methanol etch for 2 minutes, the second sample was treated in NH_4F/H_2O_2 for three minutes, and the third sample was treated in NH_4F/H_2O_2 for ten minutes. We varied the tilt of each sample to acquire composition variation information as a function of depth. The Bromine/Methanol sample did show a small amount of oxygen on it without a shift in the Cd, Zn, or Te peaks. There are some small carbon peaks at higher and lower binding energies, which indicate that some of the carbon on the surface is from oil contamination. There is more Te on the surface of the dielectric layer than in the bulk, and the amount of Cd increases from the surface of the dielectric layer into the bulk of the dielectric layer. The amount of oxygen also increases from the surface of the dielectric layer into the bulk of the dielectric layer. Carbon decreases from the surface of the dielectric layer in to the bulk of the dielectric layer. The sharp decline in carbon indicates that the carbon is present primarily as a surface layer. The carbon peak did not produce a binding energy shift, which indicates that the carbon on the surface is in an elemental state.

XPS data indicates that there is a surface layer composed primarily of TeO_2. This surface layer of TeO_2 is covered by an elemental layer containing several monolayers of carbon. Going further into the dielectric layer, there is an increasing appearance of CdO with a corresponding decreasing appearance of TeO_2. The oxygen trend follows the cadmium indicating that most of the oxide in the bulk of the dielectric layer is composed of CdO. A small amount of ZnO was detected, but it exists deeper into the bulk.

X-ray Auger Electron Spectroscopy (XAES) was performed in conjunction with XPS and the results are consistent with the AES data shown in the previous section. XAES data showed shifts of peaks for the elemental constituents of CZT to lower kinetic energies, with a corresponding change in the shape of the XAES peaks. The shift and the change in shape of the XAES peaks with the appearance of an oxygen peak indicates that the elemental constituents of CZT have changed their chemical state and have formed chemical bonds with oxygen.

3.3 CURRENT-VOLTAGE MEASUREMENTS

Pure 10% wt. H_2O_2 High Resistivity Material

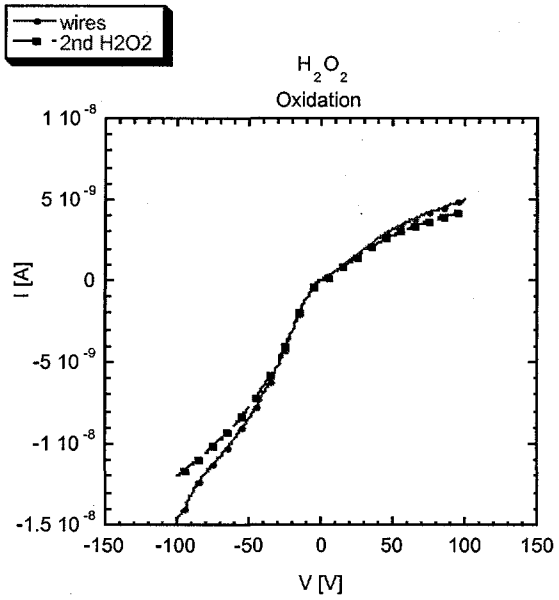

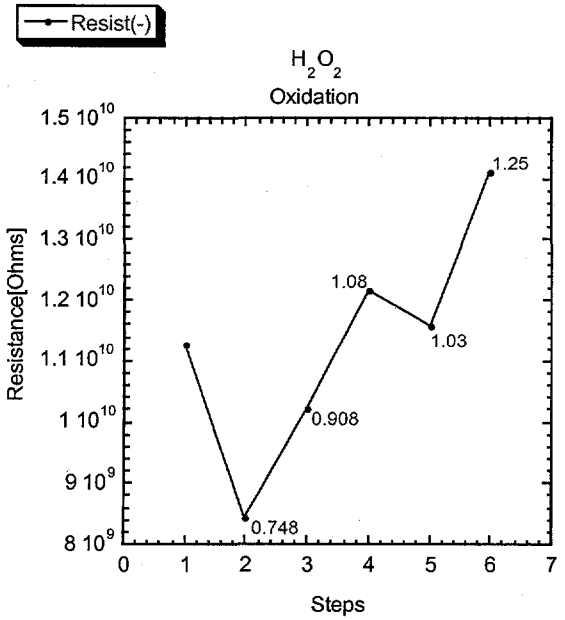

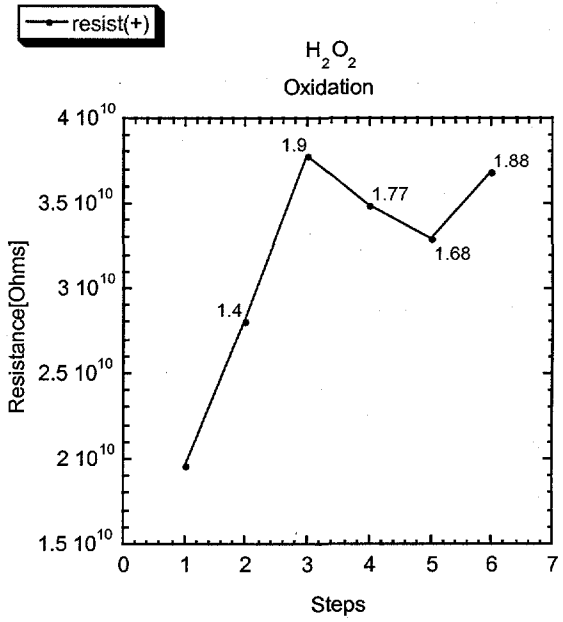

	Processing Steps	Resistance [Ohms]	Leakage Current @ 100V in [A]
1	no wires	1.13×10^{10}	-1.32×10^{-8}
2	Wires	8.42×10^{9}	-1.46×10^{-8}
3	1st Dip 5 min	1.02×10^{10}	-1.32×10^{-8}
4	2nd Dip 10 min	1.21×10^{10}	-1.20×10^{-8}
5	3rd Dip 15 min	1.16×10^{10}	-1.21×10^{-8}
6	Dry 30 min 60C°	1.41×10^{10}	-9.91×10^{-9}

	Processing Steps	Resistance [Ohms]	Leakage Current @ 100V in [A]
1	no wires	1.96×10^{10}	6.3534×10^{-9}
2	Wires	2.81×10^{10}	4.9598×10^{-9}
3	1st Dip 5 min	3.78×10^{10}	4.0884×10^{-9}
4	2nd Dip 10 min	3.48×10^{10}	4.2684×10^{-9}
5	3rd Dip 15 min	3.29×10^{10}	4.4008×10^{-9}
6	Dry 30 min 60C°	3.69×10^{10}	3.9228×10^{-9}

Figure 3.3 Current Voltage plots included with calculated resistance measurements and leakage current at negative and positive 100 Volts for each processing step. Red numbers in Resistance vs Processing Steps graph indicate the factor of improvement in resistance given by the final resistance divided by the initial resistance.

10% wt. NH_4F and 10% wt. H_2O_2 Low Resistivity CZT Material

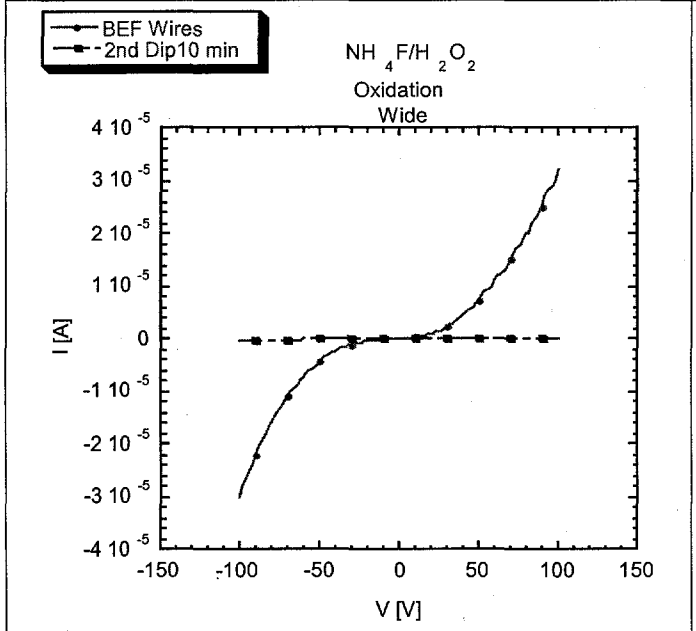

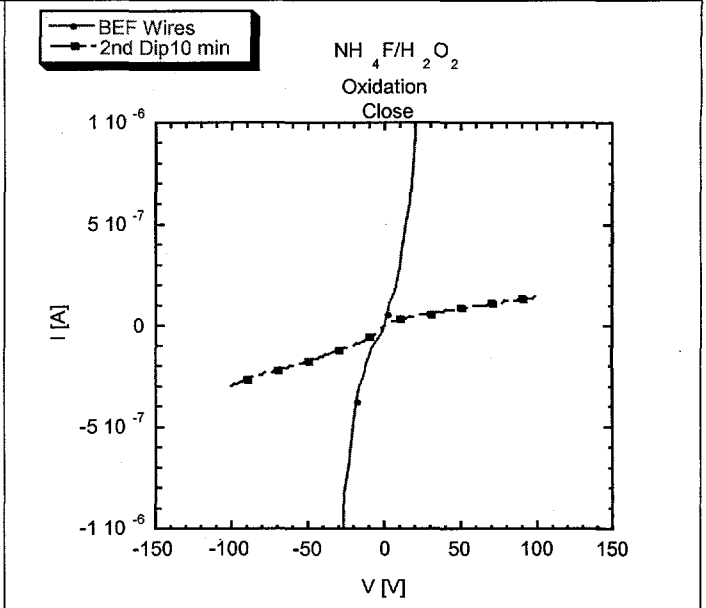

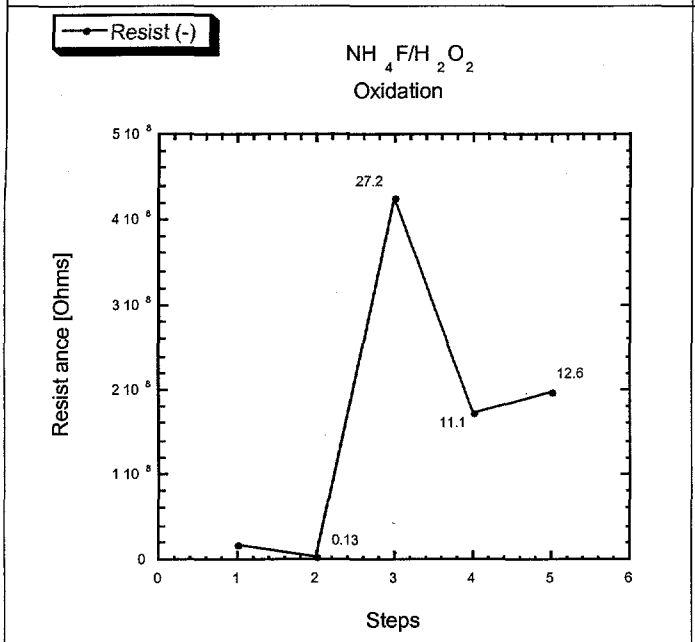

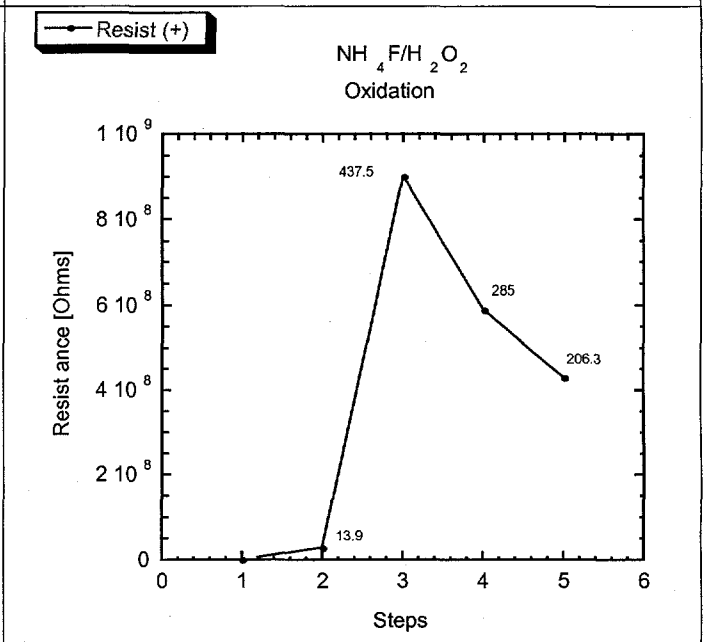

	Processing Steps	Resistance [Ohms]	Leakage Current @ 100V in [A]
1	Wires	2.06×10^{6}	-3.00×10^{-5}
2	1st Dip 5 min	2.07×10^{7}	-3.98×10^{-6}
3	2nd Dip 10 min	9.02×10^{8}	-3.01×10^{-7}
4	3rd Dip 15 min	5.08×10^{8}	-5.62×10^{-7}
5	4th Dip 15 min	4.25×10^{8}	-5.02×10^{-7}

	Processing Steps	Resistance [Ohms]	Leakage Current @ 100V in [A]
1	Wires	1.57×10^{6}	3.2000×10^{-5}
2	1st Dip 5 min	2.00×10^{7}	2.1003×10^{-6}
3	2nd Dip 10 min	4.29×10^{9}	1.4242×10^{-7}
4	3rd Dip 15 min	1.73×10^{8}	2.9740×10^{-7}
5	4th Dip 15 min	1.98×10^{8}	3.4337×10^{-7}

Figure 3.4 Current Voltage plots included with calculated resistance measurements and leakage current at negative and positive 100 Volts for each processing step. Red numbers in Resistance vs Processing Steps indicate the factor of improvement in resistance given by the final resistance divided by initial resistance.

The resistance was calculated by first applying a linear fit to the I-V curves to obtain the slope, then taking the inverse of the slope to obtain the resistance.

Table 1 Comparison of experimental results obtained with different CZT materials

Passivation Following Etching in Br/MeOH	Initial Resistance [Ω] R_I	Final Resistance [Ω] R_f	Factor of Increase in R (R_f/R_i)	Initial Leakage Current [nA] I_I	Final Leakage Current [nA] I_f	% Reduction of Leakage Current
H_2O_2 High Resistance Material (prior art)	2.81×10^{10}	3.78×10^{10}	1.35	4.96	4.1	19
NH_4F/H_2O_2 Low resistance Material	2.06×10^{6}	9.02×10^{8}	437	3.2×10^{4}	142	99.6

3.4 DETECTOR SPECTRA

We have used the results of CZT detector testing to assess the effectiveness of our passivation technique. A commercial nuclear spectroscopic electronic chain consisting of a preamplifier, shaping amplifier and multi-channel analyzer was used to measure the detector performance. We first tested a CZT detector, fabricated with electroless Au contacts, before any passivation attempts. The effective resistivity of this detector was too low to sustain an electric field high enough for spectrometer operation without excessive noise. The maximum electric field which could be applied, without noise saturation in the readout electronics was, 300V/cm. The leakage current was only 1 nA at this electric field but any increase in the field caused a superlinear increase in the leakage current, which saturated the electronics. Figure 3.5 shows the pre-passivation spectrum in which the effects of the low electric field can be seen. The low energy x-rays 14-21 keV are all broadened into a single peak which is narrowly separated from the zero channel noise, and the position of the 59.5 keV peak is about a factor of two lower than the position expected for full charge collection. This device was considered "non-operating" in terms of spectroscopic performance and would normally be rejected as a detector.

We next applied the passivation procedure by three successive treatments of NH_4F/H_2O_2 at five minute processing times. The detector was blown dry with N_2 and annealed at 70 ^{o}C for 10 minutes between each treatment.

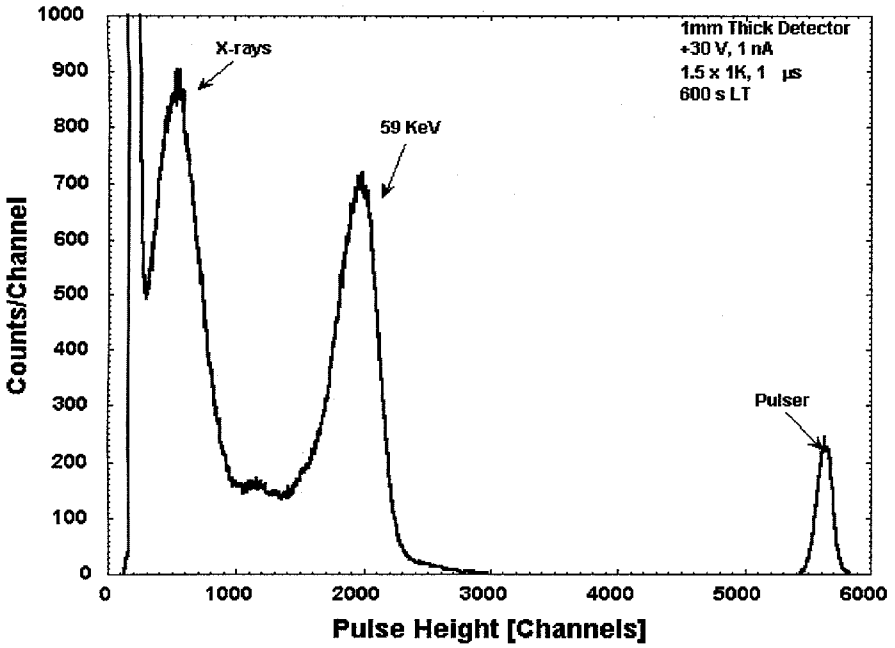

Figure 3.5 Spectrum of Am^{241} obtained with a CZT detector before NH_4F/H_2O_2 passivation.

Figure 3.6 shows the energy spectrum after surface passivation. We are able to observe improved energy resolution for all energies (X-rays and gamma rays) incident on the device demonstrating the effectiveness of the passivation agent. Overall, the device performed quite well after passivation by NH_4F/H_2O_2 treatment with increases in energy resolution, efficiency of photopeaks, and peak-to-valley counts were observed after passivation (see Table II)

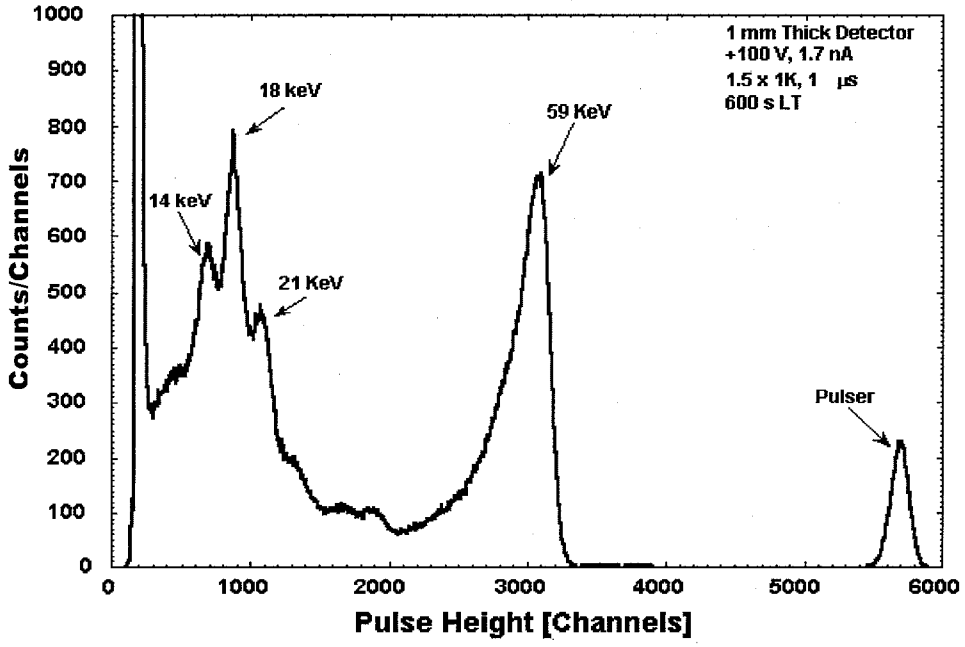

Figure 3.6 Spectrum of Am241 obtained with a CZT detector after NH_4F/H_2O_2 passivation

The post-passivated performance was significantly improved over the original performance as shown in Figure 3.6. An electric field of 1000V/cm was applied to the device, producing a leakage current of 1.7nA. Although the applied electric field is somewhat low, the improvement in charge collection causes a dramatic increase in the spectroscopic performance. First, an equivalent level of electronic noise is present even though the electric field has been increased significantly. Also,

the separate x-ray peaks (14 keV, 18 keV, and 21 keV) are now clearly resolved in the spectrum. Additionally, the position of the 59.5 keV photopeak is closer to the predicted position of approximately 4500 channels.

Table 2 Summary of CZT Detector Results After Treatment with NH_4F/H_2O_2 treatment.

NH_4F/H_2O_2	Peak:Valley ratio @ 59keV	FWHM @ 59keV	$R=\frac{FWHM}{H_o}$ X100%	$r=\frac{\text{counts @ } H_o}{\text{total counts in peak}}$ X 100%
Before	5.4 : 1	422	20.9	.22
After	13.6 : 1	269	8.7	1.2

Through this example, we have shown that a device originally useless as a low-energy radiation spectrometer can be utilized as a radiation detector through a simple passivation process. Similar results have been obtained where devices having suboptimal but adequate performance.

4.DISCUSSION

We believe that the hydrogen peroxide oxidizes the ammonium fluoride to hyponitorous acid ($H_2N_2O_2$), fluorine gas (F_2), and difluorine oxide gas (F_2O). We believe the hyponitrous acid is a much more effective oxidizing agent than H_2O_2. It is also believed that ammonium fluoride dissociates to ammonia and hydrogen fluoride ions. The fluoride ions aid in the formation of fluoride compounds from the elemental constituents of CZT, namely CdF_2, ZnF_2, TeF_4, and TeF_6. These constituent fluorides are easier to oxidize than pure CZT, and therefore allow for the formation of constituent oxides of CZT at a faster rate. It should also be noted that TeF_6 at room temperature exists as a gas and allows for a possible way to deplete excess Te from the surface.

The physical/chemical process affords a dielectric layer that is primarily composed of CdO as evidenced by the AES depth profile. The surface of the CdO layer has a layer of TeO_2 resulting from the outdiffusion of TeF_6 gas and TeF_4 ions through the initial CdO layer. The outdiffusion of TeF_6 allows for the indiffusion of O^{2-} provided by the indiffusion of water molecules or hydrogen peroxide. The indiffusion of O^{2-} is facilitated by the concentration gradient produced by the displacement of TeF_6, and possibly Te^{2-} molecules from the CZT surface. We also observe a dielectric layer consisting primarily of CdO instead of the $CdTeO_3$ reported in the literature.[9] The NH_4F/H_2O_2 treatment forms a relatively thick dielectric layer on the surface of a CZT crystal that is about 300-450 Å thick and is comprised initially of CdO with an outside layer of TeO_2. The actual thickness of the layer was difficult to accurately measure using a Dektak II surface profilometer. It is likely that some amount of the CZT surface is consumed during the oxidizing process.

5. CONCLUSIONS

A new dielectric layer was formed on CZT as evidenced by the change in electrical properties of the surface. Immersion of CZT into NH_4F/H_2O_2 produced an oxide that is much thicker than pure H_2O_2 treatments. It resulted in a color change of the surface. This oxide could potentially be utilized to develop MOSFET and MIS devices from CZT. The dielectric layer formed by the NH_4F/H_2O_2 was hard and difficult to remove. The oxide layer is thick enough to consume the nonstoichiometric surface layer on the CZT sample produced by the device processing. More importantly, the electrical properties of the oxide extend the operational parameters of the CZT detector, allowing higher bias to be applied to the detector, resulting in greater charge collection without increased noise and spectral broadening.

In summary, the addition of ammonium fluoride into a solution of hydrogen peroxide produces a dielectric layer that is ~300-450Å thick with a reduction in leakage current of up to 99%. Ellipsometry and reflection measurements are scheduled in the near future to better characterize this film's optical properties. The reduction in surface leakage current is unmatched by previous wet chemical or dry chemical treatments. Pure hydrogen peroxide solution was unable to produce comparable passivation characteristics. Therefore, we believe that ammonium fluoride in hydrogen peroxide should be utilized as a replacement for hydrogen peroxide passivation.

6. ACKNOWLEDGMENTS

The work at Fisk was supported by DOE through contract number DE-FG08-98NV13407 and by NASA through the Fisk Center for Photonic Materials and Devices, Grants NCC8-133, NCC8-145, and NCC5-286. The U.S. Department of Energy Office of Nonproliferation and National Security (DOE/NN-20) supported the work at Sandia National Laboratories CA, a multiprogram laboratory operated by Sandia Corporation, a Lockheed Martin Company, for the United States Department of Energy under contract number: DE-AC04-94AL85000.

7. REFERENCES

1) Y. Nemirovsky, and G.Bahir, J. Vac. Sci. Techn. A Vol 7 (1989) 450-452
2) R. D. Feldman, R. L. Opila, and P.M. Bridenbaugh, J. Vac. Sci. Techn. A, Vol 3, pp. (1985) 1989-1990
3) Z. Sobiersierski, I. M. Dharmadasa, and R. H. Williams, Appl. Phys. Lett., Vol 53, (1988) 2625
4) Y. Nemirvosky, J. Vac. Sci. Technol. A, Vol. 8, (1990) 1185-1187
5) A. Ruzin and Y. Nemirovsky, Appl. Phys. Lett. 71 (15), (1997) 2214
6) F. A. Ponce, R. Sinclair, and R. H. Bube, Appl. Phys. Lett., Vol. 39 (1981) 951-953
7) J. G. Werthen, J-P Haring, A. L. Fahrenbruch, and R. H. Bube, J. Appl. Phys. Vol. 54 (1983) 5986
8) F. Wang, A. l. Fahrenbruch, and R. H. Bube, J. Appl. Phys, Vol. 65, (1989) 3558
9) K-T Chen, D.T. Shi, H. Chen, B. Grandeson, M. A. George, W. E. Collins, and A. Burger and R. B. James, , J. Vac. Sci. Techn. A., 15, (1997) 850-853
10) I. Villlegas, and J. L. Stickney, J. Electrochem. Soc., Vol. 138, (1991) 1310-1319
11) Card, H. C. and Rhoderick, E. H., J. Phys. D: Appl. Phys., Vol. 4, (1971a) 1589
12) Card, H. C. and Rhoderick, E. H., J. Phys. D: Appl. Phys., Vol. 4, (1971b) 1602